Chemical Engineering Journal 165 (2010) 728–734

Contents lists available at ScienceDirect

Chemical Engineering Journal

journal homepage: www.elsevier.com/locate/cej

Rapid and cost-effective method for synthesizing zirconium silicides

Il-Je Cho[a,b], Kyung-Tae Park[c], Sang-Ki Lee[c], Hayk H. Nersisyan[d], Yong-Soo Kim[b], Jong-Hyeon Lee[c,*]

[a] Department of Nuclear Fuel Cycle System Engineering, Korea Atomic Energy Research Institute, 1045 Daedeok-daero, Yuseong-gu, Daejeon 305-353, Republic of Korea
[b] Department of Nuclear Engineering, Hanyang University, 17 Haengdang-Dong, Sungdong-Gu, Seoul 133-791, Republic of Korea
[c] Graduate School of Green Energy Technology and Department of Nano Materials Engineering, Chungnam National University, 79 Daehak-ro, Yuseong-gu, Daejeon 305-764, Republic of Korea
[d] Rapidly Solidified Materials Research Institute, Chungnam National University, 79 Daehak-ro, Yuseong-gu, Daejeon 305-764, Republic of Korea

ARTICLE INFO

Article history:
Received 5 August 2010
Received in revised form
15 September 2010
Accepted 24 September 2010

Keywords:
Zirconium silicide
Nuclear industry
Combustion synthesis
Microstructure
Phase composition

ABSTRACT

An experimental study on the preparation of zirconium silicides was conducted using $ZrSiO_4$–Mg, $ZrSiO_4$–SiO_2–Mg and $ZrSiO_4$–ZrO_2–Mg powder mixtures by the combustion synthesis (CS) technique. Test specimens having different composition ratios including Zr:Si = 1:2, 1:1, 5:4, 5:3, 2:1, and 3:1 were employed in this study. Temperature profiles relative to all the starting compositions were measured using thermocouples, and the values of the combustion parameters (combustion temperature and wave velocity) were estimated using the same. The formation of ZrSi, $ZrSi_2$, Zr_5Si_3, and Zr_3Si_2 phases was confirmed by X-ray analysis; however, only ZrSi was produced as a single-phase product. The proposed method was also extended to synthesize spherical ZrSi particles having mean diameters of 0.2–3.0 μm. A comprehensive chemical pathway to describe the sequence of chemical reactions in the combustion wave was also proposed.

1. Introduction

Transition metal silicides are hard, inert, and have high electrical and thermal stability [1]. Silicides are generally unaffected by strong acids including aqua regia. Their resistance to oxidation, particularly at high temperatures, is largely due to the formation of a tenacious oxide layer that passivates the surface to further attack [2,3]. Among silicides, zirconium silicides can be considered to be promising as future materials for the nuclear industry. Zirconium is commonly used as a cladding material for nuclear reactors because of its ultra-high neutron capture cross sections that significantly reduce neutron fields in a reactor, thus reducing reactivity and creating a barrier between the fuel pellets and the coolant [4]. The combination of zirconium with silicon has also been found to be promising for use as a neutron reflector in next-generation nuclear systems such as gas-cooled fast reactors. In such reactors, the reflector drives neutrons generated by nuclear reactions back to the core, thus improving the reactor's performance and preventing irradiation damage to outer structural compounds. Simulation based on the elastic scattering cross sections of zirconium and silicon suggests that these are among the most promising elements; however, because of their low melting point, they are not suitable for use in gas-cooled reactor cores (where temperatures could reach 2273 K under incidental conditions). An attractive solution to overcome this limitation is to combine zirconium and silicon into zirconium silicides (Zr_2Si, Zr_3Si, Zr_5Si_3, Zr_5Si_4, ZrSi, and $ZrSi_2$), some of which have fusion points of around 2473 K. However, apart from $ZrSi_2$, which unfortunately melts at 1893 K, other zirconium silicides are not commercially available.

Various processing routes have been reported for synthesizing zirconium silicides; these include the following:

- Silicothermic reduction of zirconium dioxide in vacuum at high temperatures (1473–1773 K) [5]. It has been established that silicothermic reduction in graphite furnaces can yield only the silicides $ZrSi_2$ and ZrSi. The lower-silicon phases Zr_5Si_3 and Zr_2Si cannot be produced by this technique.
- Electrochemical synthesis from molten mixtures of alkali metal fluorosilicates with oxides and fluorides of zirconium [6]. The electrosynthesis of zirconium silicides was carried out at T = 973–1023 K and almost all silicide phases were obtained.
- Mechanochemical synthesis [7] using zirconium and silicon powders as raw materials. This method produces only small quantities of silicide powder (approximately 5 g); this is unsuitable for industrial-scale use.
- Reaction sintering of zirconium and silicon powders. This method produces a ZrSi matrix containing embedded shell-like domains of Zr, Zr_2Si, and $ZrSi_2$ [8]. Other silicides (Zr_3Si_2, Zr_5Si_4, Zr_5Si_3, and Zr_3Si) hardly appear after long heat treatments.

* Corresponding author. Tel.: +82 42 821 6596; fax: +82 42 822 5850.
E-mail address: jonglee@cnu.ac.kr (Jong-Hyeon Lee).

1385-8947/$ – see front matter © 2010 Elsevier B.V. All rights reserved.
doi:10.1016/j.cej.2010.09.038

- Solid-state metathesis reactions between transition metal oxides and alkali earth metal silicides to produce transition metal disilicides and alkali earth metal oxides [9].
- Self-propagating high-temperature synthesis (SHS) using an initial mixture of Zr–αSi ($0.4 \leq \alpha \leq 2.4$) to produce all intermetallic compounds in the Zr–Si system [10,11].

Among the abovementioned processes, SHS (also called combustion synthesis, CS) is energy efficient and fast, and it can be considered to be promising for the large-scale production of zirconium silicides. SHS of zirconium silicides was first carried out by Sarkisyan et al., by burning the compacted pellets of a Zr–αSi mixture ($0.4 \leq \alpha \leq 2.4$) in an inert atmosphere [10]. The formation of Zr_2Si, Zr_5Si_3, ZrSi, and $ZrSi_2$ phases in the combustion wave was revealed by X-ray analysis, but only the $ZrSi_2$ phase was obtained in a single-phase form. Later on, a detailed kinetic study of a Zr–αSi system was conducted by Bertolino et al. [11]. The authors measured the temperature profiles in the combustion wave using an array pyrometer technique and determined the apparent activation energy relative to the propagation process. The synthesis parameters were studied as well, to reveal the synthesis conditions for zirconium silicides.

Although the combustion synthesis of zirconium silicides has its advantages, the use of the element powder makes the process cost inefficient and thus, it may not be commercially viable. Therefore, the synthesis of zirconium silicides in a more cost-effective manner, using low-cost raw materials such as $ZrSiO_4$, ZrO_2, and SiO_2 has generated great interest in the field of intermetallic compounds.

In the present study, the combustion process in $ZrSiO_4$–Mg, $ZrSiO_4$–ZrO_2–Mg, and $ZrSiO_4$–SiO_2–Mg complex systems was investigated by using the thermocouple technique to elucidate the perspectives on the synthesis of zirconium silicide powders with controlled morphology.

2. Experimental

$ZrSiO_4$ powder (64% ZrO_2; particle size, $\leq$45 μm; Junsei Chemicals Co., Ltd., Japan), Mg powder (99% purity; particle size, 50–150 μm; Daejung Chemical and Metals Co., Ltd., Republic of Korea), ZrO_2 powder (99% purity; particle size, $\leq$1.0 μm; Grand Chemical and Materials Co., Ltd., Republic of Korea), SiO_2 powder (98% purity; particle size, $\leq$45 μm; Junsei Chemicals Co., Ltd., Japan) and NaCl powder (99.5% purity; particle size $\leq$120 μm; Samchun Pure Chemicals Co., Ltd., Republic of Korea) were used as starting materials. In the proposed process, zirconium silicide powders are produced by the magnesiothermic reduction of $ZrSiO_4$ (or $ZrSiO_4$–ZrO_2 and $ZrSiO_4$–SiO_2 mixtures) followed by the acid leaching of the reduced mass to separate Mg-containing reaction by-products from the zirconium silicides. For each sample, the starting materials were weighed to target stoichiometries corresponding to the zirconium silicides, e.g., ZrSi (T_{melt} = 2483 K), $ZrSi_2$ (T_{melt} = 1893 K), Zr_5Si_4 (T_{melt} = 2523 K), Zr_3Si_2 (T_{melt} = 2488 K), Zr_5Si_3 (T_{melt} = 2453 K), and Zr_2Si(2020 K). Mixing was carried out using a ball-mill system in a polymer bottle with zirconia balls.

In a typical experiment, a cylindrical sample (diameter, 4 cm; height, 10–12 cm) was prepared from the initial reaction mixture. Then, the sample was placed in a high-pressure reactor, and combustion was carried out in argon atmosphere of 2.5 MPa to prevent the evaporation of Mg. After the local ignition of the sample by using a resistivity-heated nickel–chromium wire, a combustion wave formed and propagated steadily from the top to the bottom of the sample, converting the initial mixture into the final product. During the combustion process, a data acquisition system (GL200A, Graphtec Co., JAPAN) continuously recorded the time histories of two tungsten–rhenium thermocouples (W/Re-5 versus W/Re-20; diameter, 100 μm) previously inserted into the reaction pellet for temperature measurements. The combustion parameters examined were the combustion temperature (T_c) and combustion wave velocity (U_c). The combustion velocity was calculated as $U_c = l/t$ (where t is the time interval between temperature profiles and l, the distance between the thermocouples). After combustion, the burned sample was ground into a powder for acid leaching. Dilute HCl (10–15%) was used for all triturations. After treatment with acid, the remaining solids were always rinsed with distilled water and dried in vacuo.

Powder diffraction patterns were recorded using an X-ray diffractometer with Cu-Kα radiation (Siemens D5000, Germany). The powder morphology was studied using a scanning electron microscope (SEM; JSM 5410, JEOL, Japan).

3. Experimental results and discussion

3.1. Phase diagram of Zr–Si system and combustion thermodynamics

The phase diagram of the Zr–Si binary system is illustrated in Fig. 1. It shows the existence of a large number of zirconium silicide phases based upon the Zr/Si ratio: $ZrSi_2$, ZrSi, Zr_5Si_4, Zr_3Si_2, Zr_5Si_3, Zr_2Si, and Zr_3Si [12]. Most of the silicides are stable at low temperature; the notable exceptions are Zr_5Si_3, β-ZrSi, and β-Zr_5Si_4 high-temperature phases. From the combustion synthesis point of view, the most interesting concentration interval corresponds to 50–75 atomic% Zr, where zirconium-rich phases such as ZrSi, Zr_5Si_4, Zr_5Si_3, and Zr_2Si can be obtained [10,11]. It should be noted that most of the silicide phases have a narrow region of homogeneity, and therefore, the simultaneous formation of neighboring silicide phases can be expected irrespective of the synthesis technique used (including the combustion method).

The synthesis of zirconium silicide phases by the magnesiothermic reduction of $ZrSiO_4$–ZrO_2–SiO_2 system is a new task in the combustion synthesis field, and much useful information can be obtained theoretically using "THERMO," which is a thermodynamic software specifically designed for combustion processes [13]. This analysis allows the prediction of the adiabatic combustion temperature (T_{ad}) and equilibrium silicide phases under the given pressure. Fig. 2 shows the change in the adiabatic combustion temperature, T_{ad}, and mole concentration (C) of equilibrium products versus α. Here, α denotes the ratio of the Zr/Si atoms in the reaction mixture (for instance, α = 0.5 ($ZrSiO_4$–SiO_2–6Mg); α = 1.0 ($ZrSiO_4$–4Mg), α = 1.67 ($ZrSiO_4$–0.67ZrO_2–5.34Mg), α = 2.0 ($ZrSiO_4$–ZrO_2–6Mg), etc.). In all compositions the concentration of

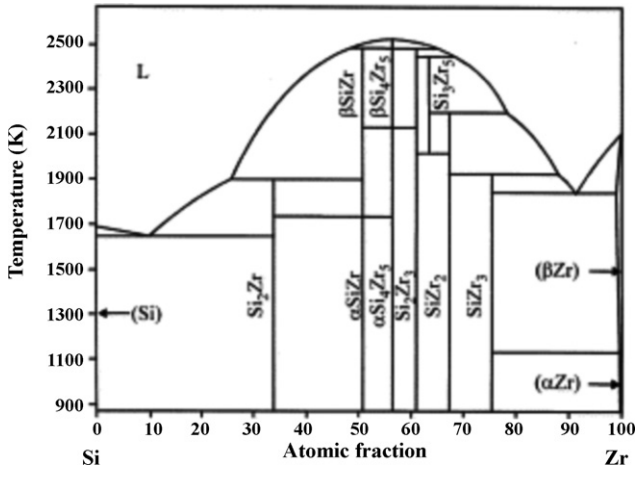

Fig. 1. Phase diagram of Zr–Si system [11].

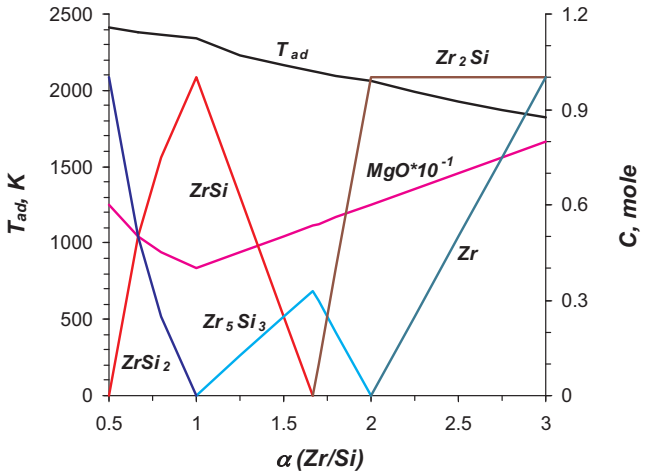

Fig. 2. Thermodynamic analysis of $ZrSiO_4$–ZrO_2–SiO_2–Mg system.

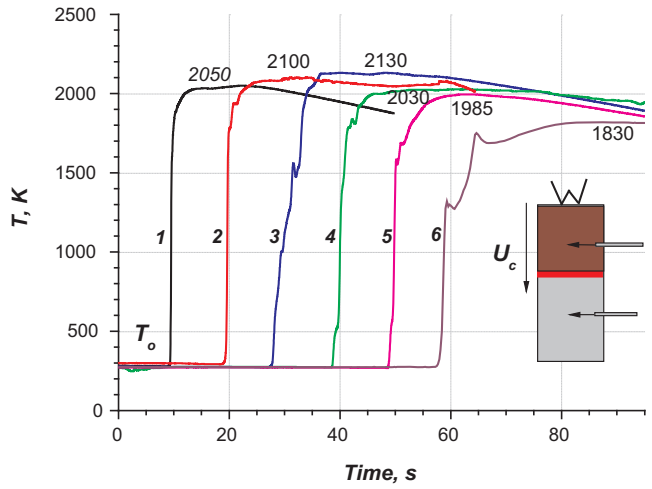

Fig. 3. Temperature–time profiles in $ZrSiO_4$–ZrO_2–SiO_2–Mg system versus α: 1 – α = 0.5; 2 – α = 1.0; 3 – α = 1.25; 4 – α = 1.67; 5 – α = 2.0; 6 – α = 3.0.

$ZrSiO_4$ was constant (1.0 mole), and the changes in the Zr/Si ratio were initiated by variations in the ZrO_2 and/or SiO_2 concentration. As seen in Fig. 1, the adiabatic combustion temperature, T_{ad}, which is maximum at α = 0.5 (2409 K), monotonously drops to reach its minimum at α = 3.0 (1823 K). At α = 0.5 (the stoichiometric point for the $ZrSi_2$ phase), the combustion product consists of $ZrSi_2$ and MgO phases. Simultaneous formation of two silicide phases (ZrSi and $ZrSi_2$) along with MgO is predicted in the 0.5 < α < 1 interval of α. At α = 1, thermodynamic analysis predicts the presence of only ZrSi and MgO phases. An increase in α from 1.0 to 1.67 leads to the formation of a new silicide phase, Zr_5Si_3, the concentration of which constantly increases with α up to its maximum at α = 1.67. At this point, the combustion product contains only Zr_5Si_3 and MgO phases. Above this point, a Zr_2Si phase also appears along with Zr_5Si_3. A pure Zr_2Si phase is predicted to be formed at α = 2. A further increase in α (α > 2) negatively affects the product composition, i.e., the formation of free Zr along with Zr_2Si and MgO phases is thermodynamically favored. Thus, the thermodynamic analysis clearly shows that four silicide phases ($ZrSi_2$, ZrSi, Zr_5Si_3, and Zr_2Si) may be obtained in the combustion wave, from the designed system, under the Mg pressure. However, single-phase silicides of zirconium are expected only in the stoichiometric points (α = 0.5, 1.0, 1.67, and 2).

3.2. Combustion synthesis

Combustion experiments were performed following the compositions corresponding to the intermetallic compounds in the binary Zr–Si system. All the reactions developed a stable self-propagating front that proceeded throughout the entire sample. Temperature profiles relative to all the starting compositions recorded using thermocouples in the sample center are shown in Fig. 3. The boundary between the preheating (left side of ordinate) and the reaction zones (right side of ordinate) is related to the melting of Mg (923 K); this initiates combustion between the reactant particles, leading to the generation of a large amount of heat within milliseconds. Therefore, the temperature sharply increases at the boundary between the preheating and the reaction zones. Most temperature profiles exhibit a small and local vibration of temperature above 1473 K. These vibrations appear to have some endothermic character and are likely associated with the melting and evaporation of reaction components such as Mg (T_{melt} = 923 K, T_{evap} = 1380 K) and SiO_2 (T_{melt} = 1920 K).

For all the compositions, the temperatures measured at the reaction front were 1830–2130 K (Fig. 4). The maximum temperature values, 2100–2130 K, were recorded for α = 1.0–1.3. In addition, in the 1.0 ≤ α ≤ 3.0 diapason of α, the combustion temperature is lower than the melting point of the corresponding silicide phases ($T_c < T_{melt}$). At α < 1.0, the combustion temperature is higher than the melting point of $ZrSi_2$ but lower than the melting point of ZrSi. Despite the high chemical activity and the large amount of magnesium in the reaction mixture, the combustion wave has a slow propagation rate, which is a major advantage of the designed system for the safe production of zirconium silicides on a large scale. As seen in Fig. 4, the combustion velocity (U_c) correspondingly changes from 0.13 to 0.18 cm/s. It is likely that the high melting point (2823 K) and relatively large size of the $ZrSiO_4$ particles (≤0.45 mm) result in low burning rates in the designed system.

3.3. Phase composition and microstructure

The XRD patterns of the acid leached products for α = 0.5, 1.0, and 2.0 are shown in Fig. 5. For the Si-rich composition (α = 0.5), the main phase is zirconium disilicide ($ZrSi_2$), the proportion of which is approximately 80%, as estimated from Fig. 5(a). In addition to $ZrSi_2$, a noticeable amount of ZrSi and unreacted Si is also present in the final product. Single-phase ZrSi was obtained from the $ZrSiO_4$–4Mg mixture (α = 1) (Fig. 5(b)). The final products for the other stoichiometries (α = 1.67, 2, and 3) were always a mixture of two silicide phases. For instance, at α = 2, the product is characterized by the high-temperature phase Zr_5Si_3 as the major component along with Zr_3Si_2 and $Mg_2Zr_5O_{12}$ phases (Fig. 5(c)). More increase

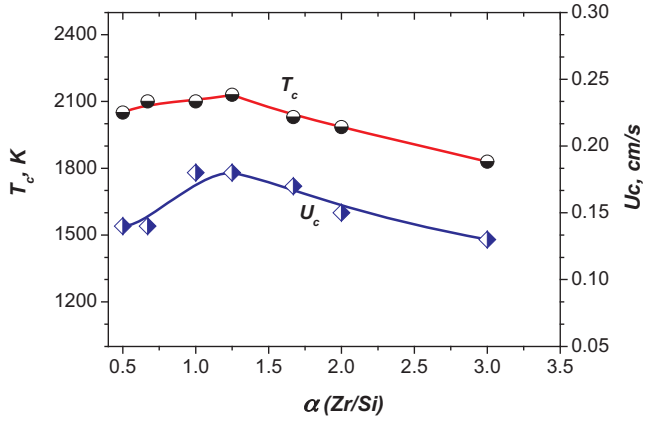

Fig. 4. Combustion parameters versus α (Zr/Si).

Table 1
Combustion parameters (T_c, U_c) and the phase composition of acid leached final products.

Initial mixture	α (Zr/Si)	T_c, K	U_c, cm/s	Phase composition
$ZrSiO_4$–SiO_2–6Mg	0.5	2050	0.14	$ZrSi_2$, ZrSi, Si
$ZrSiO_4$–4Mg	1	2100	0.18	ZrSi
$ZrSiO_4$–0.67ZrO_2–5.34Mg	1.67	2030	0.17	Zr_5Si_3, Zr_3Si_2, $Mg_2Zr_5O_{12}$
$ZrSiO_4$–ZrO_2–6Mg	2	1985	0.15	Zr_5Si_3, Zr_3Si_2, $Mg_2Zr_5O_{12}$
$ZrSiO_4$–2ZrO_2–8Mg	3	1830	0.13	Zr_3O, Zr_3Si_2, Zr_5Si_3
$ZrSiO_4$–4Mg–0.5NaCl	1	2050	0.16	ZrSi
$ZrSiO_4$–4Mg–1.0NaCl	1	1870	0.12	ZrSi
$ZrSiO_4$–4Mg + 1.5NaCl	1	1750	0.07	ZrSi

in the Zr concentration ($\alpha = 3$) results in the product being characterized by Zr_3O as the major component along with Zr_3Si_2 and Zr_5Si_3 phases (see Table 1).

The combustion synthesis of the Zr_5Si_3 high-temperature phase from Zr + αSi ($0.4 \le \alpha \le 1.0$) mixtures was first reported by Sarkisyan et al. [10]. Thereafter, N. Bertolino et al. obtained similar results by carrying out the combustion of Zr–Si pellets of 0.8 mm diameter. It was shown that the amount of ZrSi phase in the final product increases with the cooling rate: the higher the cooling rate, the larger the amount of ZrSi present in the final product. In our study, a large amount of Zr_5Si_3 phase was also recorded by X-ray analysis irrespective of the composition of the initial mixture and the relatively large diameter of the pellets (4.0 cm). Therefore, we infer that the formation of Ti_5Si_3 in the combustion wave is related not only to the fast cooling rate of the samples but is more likely to be related to the specific features of the combustion process, including fast heating and cooling rates, the specific mechanism of the combustion reaction, etc., which make the formation of the Zr_5Si_3 phase possible.

It should be noted that the product phases predicted by thermodynamic analysis (Fig. 2) are not always the same as those obtained experimentally (Fig. 5). One of the reasonable explanations is that combustion may not fully follow the equilibrium thermodynamic predictions and thermodynamic calculations can only serve as an initial guideline for interpreting the experimental results.

Fig. 6 shows several fragments of the microstructure obtained from different starting compositions. It is evident that all product particles are mostly grouped together, forming porous aggregates with a network structure (Fig. 6(a)). The size of the aggregates can vary from 5 to 100 μm depending on the combustion temperature and reaction conditions. Fig. 6(b and c) shows a magnified view of the surface morphology of the particles. It can be seen that these aggregates consist of micrometer-sized particles, and the size of the pores formed between the particles is 1–3 μm. Normally, these aggregates are brittle, and they can be easily ground into a powder. Fig. 6(d) shows the particle microstructure after milling of the acid-leached product synthesized at $\alpha = 1$ (the milling was carried out for 2–3 h in ethanol using zirconia ball media). One can see that combustion synthesized ZrSi particles have irregular shape and the size less is than 10 μm; however, some particles larger than 10 μm also exist.

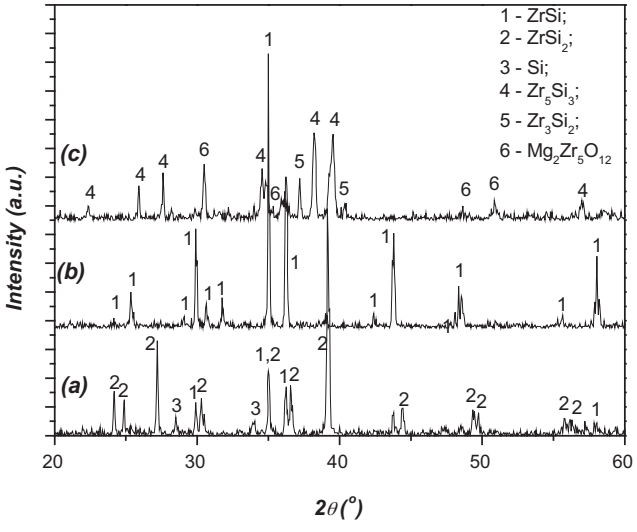

Fig. 5. XRD patterns of acid leached final products: (a) $\alpha = 0.5$, (b) $\alpha = 1.0$ and (c) $\alpha = 2.0$.

As indicated above, zirconium silicide microparticles with a textured surface were obtained after acid leaching of the combustion product. According to previous reports [14,15], the formation of a porous structure by magnesiothermic reduction is generally conditioned by the reduction of oxide phases on the surface of molten magnesium particles. The combustion process converts the $ZrSiO_4$–ZrO_2–SiO_2–Mg mixture to silicides containing multiphase aggregated particles, and acid leaching extracts secondary phases to leave a residue of porous silicide particles, as shown in Fig. 6.

3.4. Reaction pathway

The combustion process in $ZrSiO_4$–Mg, $ZrSiO_4$–ZrO_2–Mg, and $ZrSiO_4$–SiO_2–Mg systems is a complex process involving, at a minimum, reduction reactions and post-reduction processes. All three systems contain $ZrSiO_4$ and Mg as the main reaction components. ZrO_2 and SiO_2 were added to control the stoichiometry of the expected zirconium silicides. Here, we will first examine the reaction pathway in a $ZrSiO_4$–4Mg binary system.

3.4.1. $ZrSiO_4$–4Mg system ($\alpha = 1$)

The combustion process in the $ZrSiO_4$–4Mg system is highly exothermic and runs individually under a self-sustaining regime, generating a temperature of 2100 K (Fig. 3, line 2). The X-ray analysis data (Fig. 5(b)) shows that after acid leaching, the single-phase ZrSi intermetallic compound was obtained. In this system, the combustion temperature is higher than the melting and boiling points of Mg (T_{melt} = 923 K, T_{boil} = 1363 °C) but lower than the melting point of $ZrSiO_4$ (T_{melt} = 2823 K). Therefore, the chemical formula of the combustion process between $ZrSiO_4$ and Mg can be represented as follows:

$$ZrSiO_4\,(sol) + 4Mg\,(liq/gas) \rightarrow ZrSi\,(sol) + 4MgO\,(sol) \quad (1)$$

This is the basic and possibly a single-phase reaction in the $ZrSiO_4$–4Mg system, which is also responsible for the entire combustion process.

3.4.2. $ZrSiO_4$–ZrO_2–Mg system ($1 < \alpha \le 3$)

Two reduction reactions run in this system: reaction (1) and the reduction of ZrO_2 by Mg, which can be written as follows:

$$ZrO_2\,(sol) + 2Mg\,(liq) \rightarrow Zr\,(sol/liq) + 2MgO\,(sol) \quad (2)$$

According to our experiments, the combustion waves cannot run individually in the ZrO_2 + 2Mg system because of the low adiabatic temperature (T_{ad} = 1116 K), and only the combination with

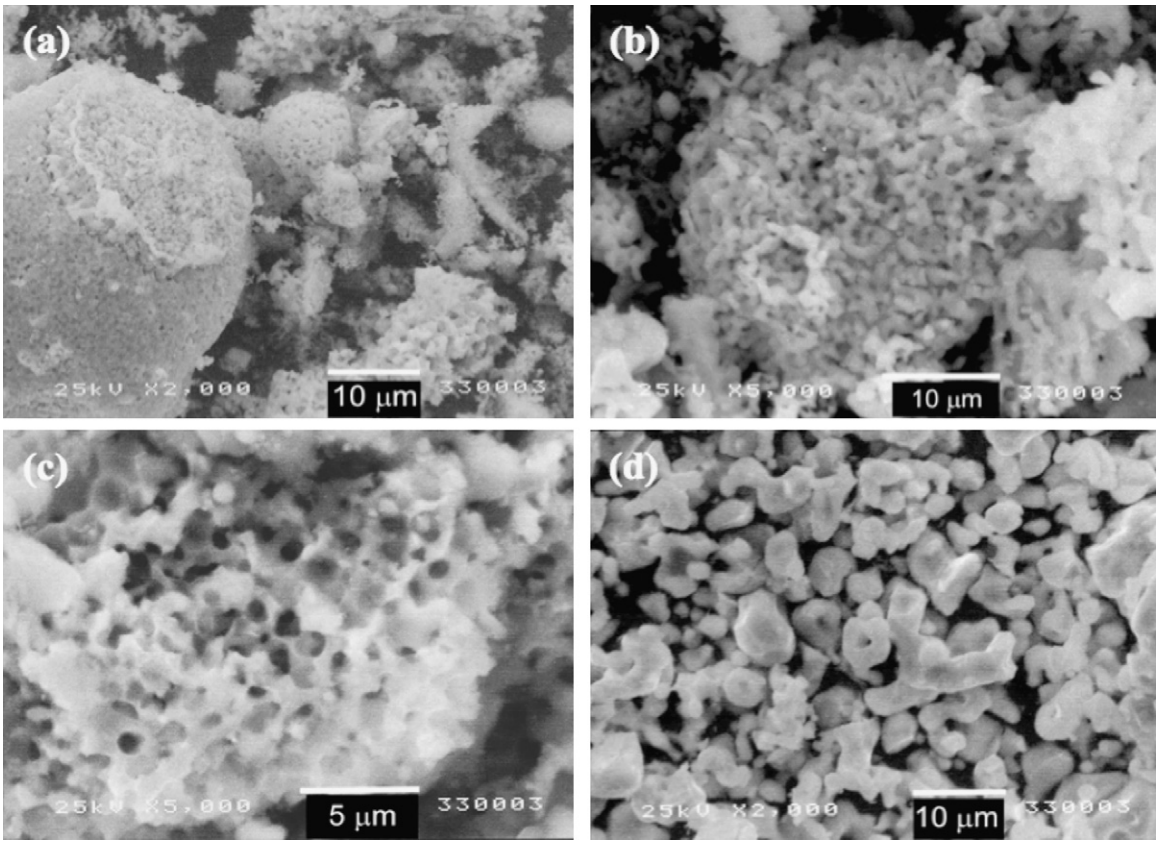

Fig. 6. Typical microstructure fragments of combustion products after acid leaching: (a) porous aggregates formed after leaching; (b and c) surface microstructure of aggregate; and (d) ground sample.

Zr_2SiO_4 thermally activates the reduction of ZrO_2. Consequently, the occurrence of reaction (2) in the combustion wave is due to heat generated by reaction (1).

The formation of the other silicides detected by X-ray analysis (Zr_3Si_2 and Zr_5Si_3) conceivably starts from ZrSi and Zr phases formed by (1) and (2). These reactions can be written as follows:

$$2ZrSi\,(sol) + Zr\,(sol/liq) \rightarrow Zr_3Si_2\,(sol) \quad (3)$$

$$3ZrSi\,(sol) + 2Zr(sol/liq) \rightarrow Zr_5Si_3\,(sol) \quad (4)$$

Some secondary reactions such as zirconium–magnesium complex oxide formation also occur in the combustion wave at $\alpha = 1.67$ and 2.0:

$$5ZrO_2 + 2MgO \rightarrow Mg_2Zr_5O_{12} \quad (5)$$

3.4.3. $ZrSiO_4$–SiO_2–Mg system ($0.5 \leq \alpha < 1.0$)

This system was designed to produce Si reach silicide of zirconium, i.e. $ZrSi_2$. The reduction stage involves reactions (1) and (6) shown below:

$$SiO_2\,(sol/liq) + 2Mg\,(liq) \rightarrow Si\,(liq) + 2MgO\,(sol) \quad (6)$$

Here, the combustion temperature is close to the melting point of SiO_2 (~1600 °C), and the reduction process occurs by liquid–liquid and solid–liquid mechanisms, resulting in the formation of elemental Si in the liquid state. This reaction has a high adiabatic temperature ($T_{ad} = 2214$ K) and can run in a self-sustaining combustion mode at room temperature. Our measurements revealed that the combustion wave of the $SiO_2 + 2Mg$ system develops a velocity of 0.35 cm/s and a temperature of 2000 K. Therefore, reduction reactions (1) and (6) are independent and run jointly. Here, the possible reaction for the formation of $ZrSi_2$ (Fig. 4(a)) can be represented as follows:

$$ZrSi\,(sol) + Si\,(liq) \rightarrow ZrSi_2\,(sol) \quad (7)$$

This is a simple and approximate reaction pathway, which cannot include all possible reactions that occur in the combustion wave. For instance, the reactions given below may also run in the $ZrSiO_4$–SiO_2–Mg system:

$$SiO_2 + Mg \rightarrow SiO + MgO \quad (8)$$

$$2SiO \rightarrow SiO_2 + Si \quad (9)$$

It seems reasonable to suppose that the ZrSi phase formed by reduction (1) serves as a "host" material to build the other silicide phases by a simple combination with Zr or Si.

At a glance, it can be seen from Fig. 4 and Table 1 that the $ZrSiO_4$–4Mg binary system has a velocity of 0.18 cm/s and a change in the velocity upon addition of SiO_2 and/or ZrO_2 occurs in the $0.12 \leq \alpha \leq 0.18$ cm/s interval. If we take into account the fact that the velocity of the $SiO_2 + 2Mg$ system is 0.35 cm/s and that the ZrO_2–2Mg system cannot propagate individually, reaction (1) becomes the best candidate for the leading process of the front propagation.

3.5. Combustion reaction in $ZrSiO_4$–4Mg–kNaCl system

We also tried to alter the combustion parameters of the $ZrSiO_4$–4Mg system in order to improve the microstructure of the ZrSi particles and to estimate the effective value of the activation energy of the combustion process. The change of the combustion parameters was realized by diluting the reaction mixture with sodium chloride (NaCl). We have previously used this procedure for the synthesis of transition metal nanopow-

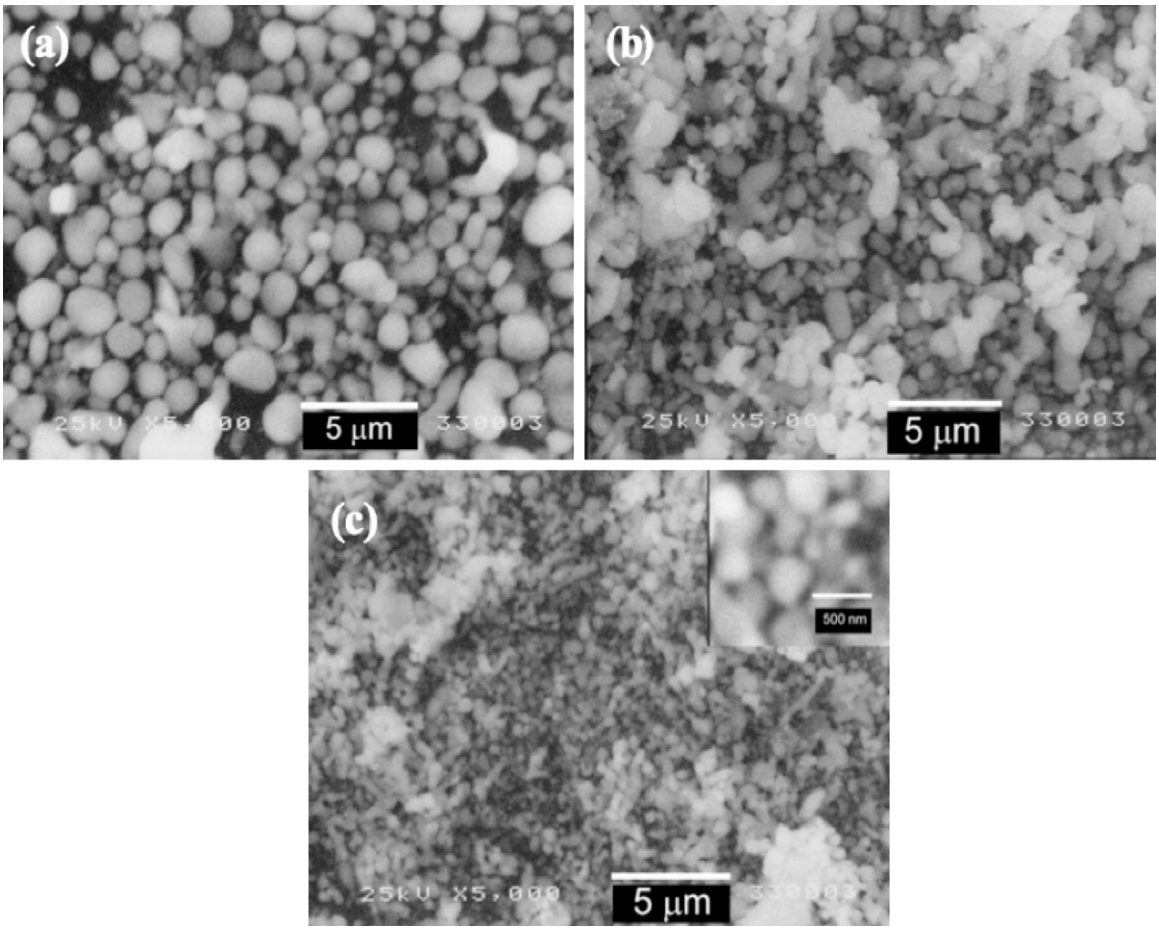

Fig. 7. Micrographs of ZrSi samples synthesized from $ZrSiO_4$–4Mg–*k*NaCl composition: (a) $k = 0.5$, (b) $k = 1.0$, and (c) $k = 1.5$.

ders by lowering the combustion temperature [16]. One can see from Table 1 that the combustion temperature is reduced from 2100 K for the undiluted sample to 1750 K for the sample with the highest level of diluent. The wave velocity correspondingly is reduced from 0.18 to 0.07 cm/s. It should be noted that the lowering of the combustion temperature did not affect the phase composition of the final product: it remained a pure ZrSi phase after acid leaching. However, SEM observations revealed a gradual change in the ZrSi microstructure: spherical particles of various sizes were obtained after adding NaCl (Fig. 7). Spherical and well-dispersed particles of ZrSi having sizes of 1–3 μm were obtained with 0.5 mole of NaCl (Fig. 7(a)). ZrSi particles having sizes of 0.5–2 μm were obtained with 1.0 mole of NaCl (Fig. 7(b)), whereas only submicrometer-sized particles of less than 500 nm were obtained with 1.5 mole of NaCl (Fig. 7(c)). It appears that ZrSi particles gradually become spherical because of the effect of the interfacial tension of the molten NaCl phase. In other words, the ZrSi phase undergoes high-temperature dissolution-precipitation processes, leaving behind the spherical particles shown in Fig. 7.

The activation energy of the $ZrSiO_4$–4Mg–*k*NaCl system associated with the combustion synthesis of ZrSi was determined using the concept proposed by Zeldovich and Frank-Kamenesky [17] and further modified by Merzhanov for SHS processes [18]. In this concept, the relation between the combustion velocity and the combustion temperature is represented by the following equation:

$$U^2 = AT_c e^{-E/RT_c} \quad (10)$$

Here, A is a constant, T_c, the combustion temperature; R, the gas constant, and E, the effective activation energy of the combustion reaction. For the calculation, the experimental values of T_c and U_c were processed in the coordinates $\ln(U_c/T_c) - 1/T_c$. The results are presented in Fig. 8. The effective activation energy of the combustion process in the $ZrSiO_4$–4Mg–*k*NaCl system was determined to be ~142.5 kJ/mol (or 34 kcal/mole). This value is similar to that calculated by Zenin et al. for the combus-

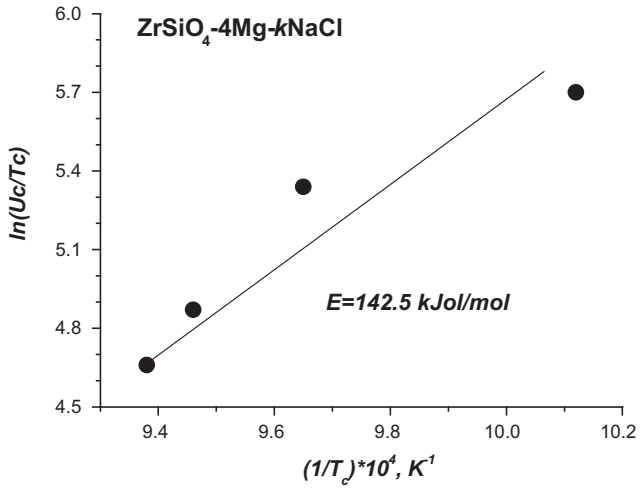

Fig. 8. Activation energy plot for reaction driving to formation of ZrSi.

tion processes [19] and somewhat higher than that reported in [11].

4. Conclusions

The combustion wave parameters (T_c, U_c) and temperature–time profiles of the $ZrSiO_4$–Mg, $ZrSiO_4$–SiO_2–Mg, and $ZrSiO_4$–ZrO_2–Mg systems were investigated to elucidate the synthesis perspectives of zirconium silicide powders with controlled morphology. For all the compositions, the temperatures measured at the reaction front were 1830–2130 K. Among the systems investigated, single-phase ZrSi was formed only in the $ZrSiO_4$–4Mg system. In the other cases, at least two silicides of zirconium were found in the combustion product. Based on XRD analysis data, an approximate reaction pathway for the formation of silicides was proposed; in this pathway, ZrSi, which was formed from the reduction of $ZrSiO_4$, served as a "host" material to build other silicides of zirconium. Adding NaCl to the $ZrSiO_4$–Mg mixture directs the combustion synthesis toward a dissolution–precipitation route, resulting in the formation of spherical and well-dispersed micro- and submicrometer-sized particles of ZrSi.

Acknowledgment

This work was supported by the Power Generation & Electricity Delivery project of the Korea Institute of Energy Technology Evaluation and Planning (KETEP) grant funded by the Ministry of Knowledge Economy of the Korean Government (No. 2010T100100392).

References

[1] L. Topor, O.J. Kleppa, Met. Trans. A 17 (1986) 1217.
[2] E.G. Rochow Jr., in: J.C. Bailar Jr., H.J. Emeleús, R. Nyholm, A.F. Trotman-Dickenson (Eds.), Comprehensive Inorganic Chemistry, vol. 1, Pergamon Press, Oxford, 1973.
[3] J.H. Weaver, A. Franciosi, V.L. Moruzzi, Phys. Rev. B 29 (1984) 3293.
[4] C. Ganguly, Advances in zirconium technology for nuclear application, in: Proceedings of the Symposium Zirconium 2002, Mumbai, 2002.
[5] A.V. Tkachenko, T.Ya. Kosolapova, Powder Metall. Metal Ceram. 7 (1968) 178–181.
[6] V.V. Malyshev, N.N. Uskova, V.I. Shapova, Powder Metall. Metal Ceram. 36 (1997) 289–292.
[7] B.K. Yen, J. Alloys Compd. 268 (1998) 266–269.
[8] J. Canel, J. Zaman, J. Bettembourg, M.L. Flem, S. Poissonnet, Int. J. Appl. Ceram. Technol. 3 (1) (2006) 23–31.
[9] A.M. Nartowski, I.P. Parkin, Polyhedron 21 (2002) 187–191.
[10] A.R. Sarkisyan, S.K. Dolukhanyan, I.P. Borovinskaya, Powder Metall. Metal Ceram. 17 (1978) 424–427.
[11] N. Bertolino, U. Anselmi-Tamburini, F. Maglia, G. Spinolo, Z.A. Munir, J. Alloys Compd. 288 (1999) 238–248.
[12] H. Okamoto, Bull. Alloy Phase Diagrams 11 (1990) 513.
[13] A.A. Shiryaev, Int. J. SHS 4 (1995) 351–359.
[14] C.W. Won, H.H. Nersisyan, H.I. Won, Chem. Eng. J. 157 (2010) 270–275.
[15] C.W. Won, H.H. Nersisyan, C.Y. Shin, J.H. Lee, Micropor. Mesopor. Mater. 126 (2009) 166–170.
[16] C.W. Won, H.H. Nersisyan, H.I. Won, J.H. Lee, Curr. Opin. Solid State Mater. Sci. 14 (2010) 53–68.
[17] J.B. Zeldovich, D.A. Frank-Kamenesky, Russian J. Phys. Chem. 12 (1938) 100–105 (in Russian).
[18] A.G. Merzhanov, Russian Chem. Bull. 46 (1997) 1.
[19] A.A. Zenin, A.G. Merzhanov, H.H. Nersisyan, Combustion, Explosion Shock Wave 1 (1981) 79–86.